Road Materials and Pavement Design

ISSN: (Print) (Online) Journal homepage: https://www.tandfonline.com/loi/trmp20

Analytical modelling of thixotropy contribution during T/C fatigue tests of asphalt concrete with the VENoL model

L. Coulon, G. Koval, C. Chazallon & J.-N. Roux

To cite this article: L. Coulon, G. Koval, C. Chazallon & J.-N. Roux (2021) Analytical modelling of thixotropy contribution during T/C fatigue tests of asphalt concrete with the VENoL model, Road Materials and Pavement Design, 22:sup1, S536-S559, DOI: 10.1080/14680629.2021.1911833

To link to this article: https://doi.org/10.1080/14680629.2021.1911833

Published online: 16 Apr 2021.

ROAD MATERIALS AND PAVEMENT DESIGN
2021, VOL. 22, NO. S1, S536–S559
https://doi.org/10.1080/14680629.2021.1911833

Taylor & Francis
Taylor & Francis Group

Analytical modelling of thixotropy contribution during T/C fatigue tests of asphalt concrete with the VENoL model

L. Coulon[a], G. Koval[a], C. Chazallon[a] and J.-N. Roux[b]

[a]ICube (CNRS UMR 7357), INSA Strasbourg, Strasbourg, France; [b]Laboratoire Navier (CNRS UMR 8205), Université Gustave Eiffel, Marne-la-Vallée, France

ABSTRACT

The classical modelling of fatigue tests carried out in the laboratory on asphalt concrete consists in predicting the decrease in the overall complex stiffness modulus. However, this approach is limited because reversible phenomena, called biasing effects (nonlinearity, self-heating and thixotropy), develop in parallel with damage. The VENoL (T,ω,ε_0) model is already able to reproduce tests of instantaneous complex stiffness modulus for different strain amplitudes. The study carried out in this paper consists of improving it by predicting the evolution of thixotropy during fatigue tests. The modelling is based on the hypothetical property that thixotropy follows the viscoelastic path of the instantaneous complex stiffness modulus. Experimental data from continuous fatigue tests in direct T/C on cylindrical specimens and taken from the literature are used. The results obtained are encouraging because they corroborate the experimentation, but only for one level of strain amplitude imposed in fatigue.

ARTICLE HISTORY
Received 31 July 2020
Accepted 26 March 2021

KEYWORDS
Asphalt concrete; complex stiffness modulus; fatigue; nonlinearity; thixotropy; VENoL model

1. Introduction

During its life, a road is subjected to repeated traffic which causes mechanical damage within the layers constituting it. To better understand this fatigue phenomenon and improve the roads design, cyclic loading tests are commonly carried out in the laboratory on bituminous mixtures specimens. There are several types of fatigue tests, the most common are: the direct tensile–compression (T/C) test on a cylindrical specimen, the two-point bending test on a trapezoidal specimen, the four-point bending test on a beam. From these tests, a typical decreasing curve of the norm of the complex stiffness modulus as a function of the number of cycles is obtained. The modulus decreases rapidly and sharply at the start (Stage I), then slowly but continuously (Stage II) before dropping sharply following the sample rupture (Stage III).

It is now recognised that the shape of this curve is not only due to irreversible damage. Some biasing effects also appear in parallel during a fatigue test and depending on the fatigue procedure used, the experimental results can be altered leading to false conclusions (Di Benedetto et al., 2004). These biasing effects are reversible because asphalt mixtures possess the capacity to recover part of their mechanical properties after stopping the test. The most common of them relating to fatigue tests are nonlinearity (when strain amplitude is raised), self-heating and thixotropy (although the last one is still a hypothesis) (Di Benedetto et al., 2011).

CONTACT L. Coulon leo.coulon@insa-strasbourg.fr

This article has been republished with minor changes. These changes do not impact the academic content of the article.

According to the International Union of Pure and Applied Chemistry (IUPAC, 1997), thixotropy is defined as

> The application of a finite shear to a system after a long rest may result in a decrease of the viscosity or the consistency. If the decrease persists when the shear is discontinued, this behaviour is called work softening (or shear breakdown), whereas if the original viscosity or consistency is recovered this behaviour is called thixotropy

A large review about thixotropy is proposed in (Mewis & Wagner, 2009). The authors resume the thixotropy mechanisms by the existence of weak attractive forces between particles which cause the formation of a flocs network. During flow, these forces are broken by the mechanical stresses. The network breaks down in separate flocs, which decrease further in size when the strain rate is increased. Reducing the shear rate can cause a growth of the flocs and arresting the flow will allow the particulate network to rebuild.

Evidence of thixotropy in asphalt binders has been repeatedly demonstrated (Babadopulos et al., 2019; Mouillet et al., 2012; Pérez-Jiménez et al., 2012; Shan et al., 2011).

Over the past two decades, several authors have searched to quantify these biasing effects, particularly thixotropy, in asphalt concrete fatigue tests. A rest period is carried out between each fatigue loop to separate biasing effects from damaging effects (Baaj et al., 2018; Botella et al., 2020; Di Benedetto et al., 2011; Isailović et al., 2017; Mangiafico et al., 2015; Phan et al., 2017a; Riahi et al., 2017). From his previous article, Phan demonstrates that the thixotropic effect seems to follow the viscoelastic path of the instantaneous complex stiffness modulus during a fatigue test.

The classical approach to model fatigue test on asphalt concrete consists in predicting the decrease in the overall complex stiffness modulus with a continuum damage approach (Baaj, 2002; Bodin et al., 2004; Castro & Sanchez, 2007; Christensen & Bonaquist, 2012; Hernandez-Fernandez et al., 2020; Hou, 2009; Lee et al., 2000; Liu, 2019; Lv et al., 2020; Underwood & Kim, 2013). Recently, several authors have attempted a different approach by searching to model separately the biasing effects depending on viscoelasticity and acting in fatigue: nonlinearity (Coulon et al., 2021b; Graziani et al., 2019; Nguyen et al., 2015; Schapery, 1969; Zeng, 1997; Zeng et al., 2001), self-heating (Riahi et al., 2017). However, to our knowledge, there is until this day no modelling of the thixotropy effect (separated from other effects) on bituminous mixtures during a fatigue test.

This study, presented after, is part of a wider research effort in the framework of a PhD thesis (Coulon, 2022), itself integrated into the national project ANR MoveDVDC. This project, which involves many partners, aims to evaluate the influence of aging and damage of asphalt concrete materials on the lifetime of road pavements.

Previous research has led to the creation of the analytical VENoL(T,ω,ε_0) model, which already makes it possible to model the instantaneous complex stiffness modulus of asphalt concrete as well as their nonlinear behaviour. This research work is extended here in order to improve the VENoL model by adding a modelling of thixotropy acting during fatigue tests. Phan's experimental data from continuous fatigue tests in direct T/C on cylindrical specimens are used and exploited again (Phan et al., 2017a). This work is presented in the following parts.

2. Principle of the VENoL(T,ω,ε_0) model

2.1. Introduction

The VENoL model, for NOn Linear ViscoElastic model, can represent the viscoelastic behaviour of a bituminous mixture by calculating the instantaneous complex stiffness modulus according to the temperature T of the environment, the pulsation (or angular frequency) ω and the strain amplitude ε_0 of the imposed signal. It was first introduced in (Coulon et al., 2021a) and improved in (Coulon et al. 2021b). His whole principle is summarised in this Section 2.

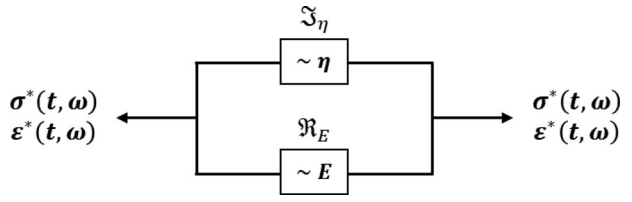

Figure 1. Schematic diagram of the VENoL model.

2.2. Design of the VENoL model

In dynamic analysis, the complex stiffness modulus $E^*(t)$ is obtained by dividing the stress signal $\sigma^*(t)$ by the strain signal $\varepsilon^*(t)$ (Equations (1)–(3)). ε_0 is the strain amplitude, σ_0, the stress amplitude and φ, the phase angle.

$$\sigma^*(t) = E^*(t) \cdot \varepsilon^*(t), \tag{1}$$

with,

$$\varepsilon^*(t) = \varepsilon_0 \cdot e^{i\cdot\omega t}, \tag{2}$$

$$\sigma^*(t) = \sigma_0 \cdot e^{i\cdot(\omega t+\varphi)}, \tag{3}$$

The stiffness modulus can split its complex form into two, composed of a real part $\Re(E^*)$ and an imaginary part $\Im(E^*)$ having for the unit the Pascal (Equation (4)). By dividing $\Im(E^*)$ by the signal pulsation ω, we obtain $\Im_\eta$ akin to a viscosity. We call it « viscosity component ». In the same way, we replace $\Re(E^*)$ by $\Re_E$ and we call it « stiffness component » (Equation (5)). The multiplication of $i\omega$ by $\varepsilon^*(t)$ gives the derived function, the strain rate $\dot{\varepsilon}^*(t)$. By analogy, the general equation naturally obtained is the same as that of the Kelvin–Voigt model (Equation (6)).

$$\sigma^*(t) = [\Re(E^*) + i \cdot \Im(E^*)] \cdot \varepsilon^*(t), \tag{4}$$

$$\sigma^*(t) = [\Re_E + i\omega \cdot \Im_\eta] \cdot \varepsilon^*(t) \tag{5}$$

$$with, \begin{cases} \Re(E^*) = \Re_E \\ \Im(E^*) = \omega \cdot \Im_\eta \end{cases},$$

$$\sigma^*(t) = \Re_E \cdot \varepsilon^*(t) + \Im_\eta \cdot \dot{\varepsilon}^*(t). \tag{6}$$

Schematically, the VENoL model can therefore be represented with two elements $\Re_E$ and $\Im_\eta$ mounted in parallel (Figure 1).

2.3. Variations of $\Re_E$ and $\Im_\eta$

The stiffness component $\Re_E$ and the viscosity component $\Im_\eta$ depend on the environment temperature T, the pulsation ω and the strain amplitude ε_0 of the imposed signal. We present hereafter a global formalism to take them into account in an analytical method.

2.3.1. TTSP principle

The Time–Temperature Superposition Principle (TTSP) makes it possible to relate temperature and pulsation. It is characterised by a translation factor a_T to calculate the reduced pulsation ω_{R-T} and the

reduced viscosity component $\Im_{\eta,R-T}$ (Equations (7) and (8)).

$$\omega_{R-T} = a_T \cdot \omega, \tag{7}$$

$$\Im_{\eta,R-T} = \frac{\Im_\eta}{a_T}, \tag{8}$$

The factor a_T is calculated with the Williams-Landel-Ferry (WLF) relation according to the temperature T (Equation (9)) (Williams et al., 1955). T_{ref} is the chosen reference temperature, $C_{1,aT}$ and $C_{2,aT}$ are two constants. The factor a_T is equal to 1.0 at T_{ref}.

$$\log a_T(T) = \frac{-C_{1,\mathrm{aT}}.(T - T_{ref})}{C_{2,\mathrm{aT}} + (T - T_{ref})}. \tag{9}$$

2.3.2. TASSP principle

The Time-Amplitude Semi-Superposition Principle (TASSP) connects strain amplitude and pulsation. It is characterised by two translation factors a_A and b_A. The factor a_A intervenes on the reduced pulsation ω_{R-A} and on the reduced viscosity component $\Im_{\eta,R-A}$ (Equations (10) and (11)). The factor b_A is a correction coefficient which only affects $\Im_{\eta,R-A}$ (Equation (11)). That is why the term semi-superposition is used.

$$\omega_{R-A} = a_A.\omega \tag{10}$$

$$\Im_{\eta,R-A} = \frac{\Im_\eta}{a_A \cdot b_A}. \tag{11}$$

We have observed that a_A and b_A seem to follow a WLF-type law according to ε_0 (Equations (12) and (13)). The use of these laws requires defining a reference amplitude $\varepsilon_{0,ref}$. $C_{1,aA}$, $C_{2,aA}$ and $C_{1,bA}$, $C_{2,bA}$ are constants. The factors a_A and b_A are equal to 1.0 at $\varepsilon_{0,ref}$.

$$\log a_A(\varepsilon_0) = \frac{-C_{1,\mathrm{aA}} \cdot (\varepsilon_0 - \varepsilon_{0,ref})}{C_{2,\mathrm{aA}} + (\varepsilon_0 - \varepsilon_{0,ref})}, \tag{12}$$

$$\log b_A(\varepsilon_0) = \frac{-C_{1,bA} \cdot (\varepsilon_0 - \varepsilon_{0,ref})}{C_{2,bA} + (\varepsilon_0 - \varepsilon_{0,ref})}. \tag{13}$$

The TASSP existence could be explained by the dependence of viscosity on velocity. The pulsation of a sinusoidal signal is indeed equal to the maximum velocity of the signal divided by its amplitude. Therefore, for a constant pulsation, increasing the amplitude leads to increase the maximum velocity.

2.3.3. TTASSP principle

The combination of the TTSP and the TASSP gives the Time–Temperature–Amplitude Semi-Superposition Principle (TTASSP). It is characterised by the translation factors a_{TA} (Equation (14)) and b_A. For the reference conditions, a_{TA} and b_A are equal to 1.0. The combination allows to calculate the reduced pulsation ω_{R-TA} (Equation (15)) and to correct the reduced viscosity component $\Im_{\eta,R-TA}$ (Equation (16)).

$$a_{TA} = a_T \cdot a_A, \tag{14}$$

$$\omega_{R-TA} = a_{TA} \cdot \omega, \tag{15}$$

$$\Im_{\eta,R-TA} = \frac{\Im_\eta}{a_{TA} \cdot b_A}. \tag{16}$$

Table 1. VENoL(T,ω,ε_0) model. Evolution of the parameters naming of the CY laws defining the stiffness and viscosity components $\Re_E$ and $\Im_\eta$ according to the principle used.

Parameters	TTSP	TTASSP
Transition reduced pulsation [rad/s]	$\omega_{R-T,tr}$	$\omega_{R-TA,tr}$
Stiffness component – Parameter 1 controlling the position of the curve on the axis ω [s/rad]	$\lambda_{E,R-T,1}$	$\lambda_{E,R-TA,1}$
Stiffness component – Parameter 2 controlling the position of the curve on the axis ω [s/rad]	$\lambda_{E,R-T,2}$	$\lambda_{E,R-TA,2}$
Viscosity component – Lower bound [MPa.s]	$\Im_{\eta,R-T,low,1}$	$\Im_{\eta,R-TA,low,1}$
Viscosity component – Parameter 1 controlling the position of the curve on the axis ω [s/rad]	$\lambda_{\eta,R-T,1}$	$\lambda_{\eta,R-TA,1}$
Viscosity component – Upper bound [MPa.s]	$\Im_{\eta,R-T,up,2}$	$\Im_{\eta,R-TA,up,2}$
Viscosity component – Parameter 2 controlling the position of the curve on the axis ω [s/rad]	$\lambda_{\eta,R-T,2}$	$\lambda_{\eta,R-TA,2}$

2.3.4. Calculation of $\Re_E$ and $\Im_\eta$ from the TTASSP

Variations of the stiffness component $\Re_E$ (green curves on Figure 2) and the reduced viscosity component $\Im_{\eta,R-TA}$ (red curves) as a function of the reduced pulsation ω_{R-TA} can be fitted using Carreau–Yasuda (CY) laws (Equations (17) and (18)), which represent sigmoid in a logarithmic coordinate system (Byron Bird & Carreau, 1968; Yasuda, 1979). The behaviour of asphalt concrete mixes varies greatly around a transition reduced pulsation $\omega_{R-TA,tr}$, which corresponds to a peak of the phase angle (blue curve). This implies to characterise a modelling below $\omega_{R-TA,tr}$ (dotted curves) and a modelling above $\omega_{R-TA,tr}$ (continuous curves). Therefore, four fits with CY laws are needed, defined with the next parameters: $\Re_{E,low,1}$, $\Im_{\eta,R-TA,low,1}$ and $\Re_{E,up,2}$, $\Im_{\eta,R-TA,up,2}$ [MPa, MPa.s] are respectively lower and upper bounds, λ [s/rad] controls the position of the curve on the axis ω, n [–] is a slope coefficient and k [–] a slope/bound transition coefficient. These parameters are calibrated for the reference curves with the conditions T_{ref} and $\varepsilon_{0,ref}$.

$$\Re_E(T,\omega,\varepsilon_0) = \begin{cases} \text{if } \omega_{R-TA} \le \omega_{R-TA,tr}, \\ \Re_{E,low,1} \cdot [1 + [\lambda_{E,R-TA,1} \cdot \omega_{R-TA}]^{k_{E,1}}]^{\frac{n_{E,1}-1}{k_{E,1}}} \\ - \\ \text{if } \omega_{R-TA} \ge \omega_{R-TA,tr}, \\ \Re_{E,up,2} \cdot [1 + [\lambda_{E,R-TA,2} \cdot \omega_{R-TA}]^{k_{E,2}}]^{\frac{n_{E,2}-1}{k_{E,2}}} \end{cases}$$

$$k_{E,1} > 0; n_{E,1} > 1; k_{E,2} < 0; n_{E,2} > 1, \tag{17}$$

$$\Im_{\eta,R-TA}(T,\omega,\varepsilon_0) = \begin{cases} \text{if } \omega_{R-TA} \le \omega_{R-TA,tr}, \\ \Im_{\eta,R-TA,low,1} \cdot [1 + [\lambda_{\eta,R-TA,1} \cdot \omega_{R-TA}]^{k_{\eta,1}}]^{\frac{n_{\eta,1}-1}{k_{\eta,1}}} \\ - \\ \text{if } \omega_{R-TA} \ge \omega_{R-TA,tr}, \\ \Im_{\eta,R-TA,up,2} \cdot [1 + [\lambda_{\eta,R-TA,2} \cdot \omega_{R-TA}]^{k_{\eta,2}}]^{\frac{n_{\eta,2}-1}{k_{\eta,2}}} \end{cases};$$

$$k_{\eta,1} < 0; n_{\eta,1} < 1; k_{\eta,2} > 0; n_{\eta,2} < 1, \tag{18}$$

If only the TTSP is used, the names of parameters resulting from the CY laws defining the stiffness and viscosity components $\Re_E$ and $\Im_\eta$ evolve but their values remain the same since a_{TA} and b_A are equal to 1.0 at the reference curve (Table 1).

2.4. Advantages and disadvantages of the VENoL model

The VENoL(T,ω) model has been built for a use with dynamic loadings. With eighteen parameters (including two for the TTSP), it can accurately reproduce the entire frequency spectrum of the complex

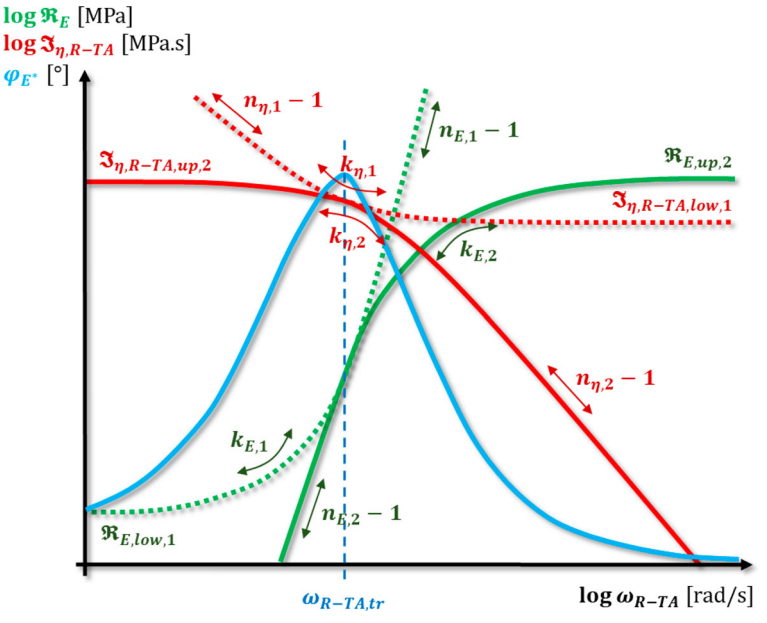

Figure 2. Illustration of variations of the stiffness component $\Re_E$ and the reduced viscosity component $\Im_{\eta,R-TA}$ as a function of the reduced pulsation ω_{R-TA}. The peak of the phase angle φ_{E^*} gives the transition reduced pulsation $\omega_{R-TA,tr}$.

stiffness modulus for one strain amplitude. In comparison, the generalised Maxwell and generalised Kelvin–Voigt models require at least thirty parameters to have an equivalent accuracy. The 2S2P1D model (nine parameters) does not allow perfect modelling at high temperature and low frequency, as we can check it from this thesis (Mangiafico, 2014, Figure 4.25). Its precision would have been sufficient if it did not need fractional derivatives, which are difficult to implement in numerical simulations.

In addition, the choice of the number of parameters for the VENoL model can vary according to requirements. For example, to reproduce the behaviour of asphalt concrete above the transition reduced pulsation $\omega_{R-T,tr}$, only ten parameters are needed. With the generalised Kelvin–Voigt model, by adding a Kelvin–Voigt element, all the set of parameters must be redefined, which is not the case with the VENoL model.

From the equations of stiffness and viscosity components $\Re_E$ and $\Im_\eta$ (Equations (17) and (18)), pulsation can be isolated in order to observe the effects of strain amplitude, which is difficult with rheological models from the literature.

Based on a Kelvin–Voigt structure, the VENoL model can be easily implemented as a contact law in numerical simulations with the Discrete Element Method (DEM), because in its stress equation, the stiffness and viscosity parameters are directly equivalent to those of the Fundamental Principle of Dynamics.

3. Use of Phan's experimental data

To implement the thixotropy in the VENoL(T,ω,ε_0) model, Phan's experimental data, from direct T/C tests on asphalt concrete and published in 2017, are used (Phan et al., 2017a).

3.1. Summary description of specimens

The sinusoidal cyclic tension–compression tests developed at the University of Lyon/ENTPE were performed on cylindrical specimens with a diameter of 75 mm and a height of 150 mm. The material used was a high modulus asphalt mixture ('Enrobé à Module Élevé' in French) respecting European

standard (NF EN 13108-1, February 2007). It was produced with a 35/50 penetration grade bitumen composing 5.1% of the sample mass (and with 0% hydrated lime contents). Samples were given the name E3550-5.1-0-# with their number instead of '#'. The specimens were cored and sawn from a 600 × 400 × 150 mm slab produced by using a French wheel compactor (NF EN 12697-33 + A1, September 2007). Their void content was approximately 4% (between 3.7% and 4.3%).

3.2. Summary description of tests of data used

The complex modulus, nonlinearity and fatigue tests carried out by Phan allow to build the VENoL model step by step. Their procedures are summarised below.

Complex modulus tests (CMT) were performed on the sample E3550-5.1-0-1 at six frequencies (from 0.03 Hz to 10 Hz) and at nine temperatures (from −25°C to 52°C). In order to obtain the viscoelastic properties on a wider range, two smaller frequencies (0.003 and 0.01 Hz) were added at three temperatures higher or equal to 35°C. Strain control mode was used to conduct tests with an amplitude of 50 µm/m. The number of loading cycles was less than 50 cycles. The entire procedure is detailed in another paper of Phan (Phan et al., 2017b). These tests allow to plot the instantaneous complex stiffness modulus in the Cole–Cole space. Their analysis allows to implement the influence of temperature and pulsation in the VENoL model.

Some nonlinearity tests (NLT) were also carried out on the sample E3550-5.1-0-6. Complex modulus tests were realised at four different temperatures (8°C, 10°C, 12°C and 14°C) and for each one, four different strain amplitudes were applied (50, 75, 100 and 110 µm/m). The frequency was fixed at 10 Hz. The applied strain amplitude was increased linearly from 0 µm/m to the targeted strain amplitude during the first fifty cycles and kept constant during the next 150 cycles before stopping loading. Their analysis allows to implement the influence of nonlinearity in the VENoL model.

Three continuous fatigue tests (CFT) were performed at the following conditions: 10°C, 10 Hz (sample E3550-5.1-0-12), 6.7°C, 3 Hz (E3550-5.1-0-8) and 25°C, 10 Hz (E3550-5.1-0-7). The conditions 10°C, 10 Hz and 6.7°C, 3 Hz correspond to the same equivalent frequency from the CMTs on E3550-5.1-0-1 in order to verify if the TTSP applied to the fatigue test. The axial strain amplitude was linearly increased from 0 to 100 µm/m during the first fifty cycles (nonlinear part) before being kept constant until the end of the test. Their analysis allows to implement the influence of thixotropy in the VENoL model.

4. Results: building of the VENoL model for the Phan's asphalt concrete

4.1. Application of the VENoL model: considering the influence of T and ω

In order to reproduce the rheological behaviour of Phan's bituminous mixture, the first major step consists of implementing the mutual influence of temperature and pulsation on the complex stiffness modulus in the VENoL model. We name it the VENoL(T,ω) model.

Many graphics are presented in this part to visualise the model construction. Table 2 lists the acronyms used in the legends of charts.

Table 2. Meaning of acronyms in the graphs legends.

Acronym	Meaning
CMT	Complex Modulus Test
NLT	NonLinearity Test
CFT	Continuous Fatigue Test
TX	ThiXotropy
Exp	Experiment
Mod	Modelling
100/20/10	Test conditions 100 µm/m/20°C/10 Hz

4.1.1. Getting experimental curves $\Re_E(\omega_{R-T})$ and $\Im_{\eta,R-T}(\omega_{R-T})$ with the TTSP

From real parts $\Re(E^*)$ and imaginary parts $\Im(E^*)$ given by the CMT on the sample E3550-5.1-0-1, the stiffness and viscosity components $\Re_E$ and $\Im_\eta$ are calculated using the Equation (5). The next step consists simply to apply the TTSP using the WLF law (Equation (9)) with the following calibration: $T_{ref} = 15°C$, $C_{1,aT} = 32$, $C_{2,aT} = 213\ °C$. The transition reduced pulsation $\omega_{R-T,tr}$ is determined equal at 3.00×10^{-3}rad/s with the location of the peak of the phase angle. The application of a_T on ω and $\Im_\eta$ (Equations (7) and (8)) allows to obtain the unique experimental curves $\Re_E(\omega_{R-T})$ and $\Im_{\eta,R-T}(\omega_{R-T})$ (Figure 3). They represent the master curves for $T_{ref} = 15°C$ and $\varepsilon_{0,ref} = 50\mu m/m$.

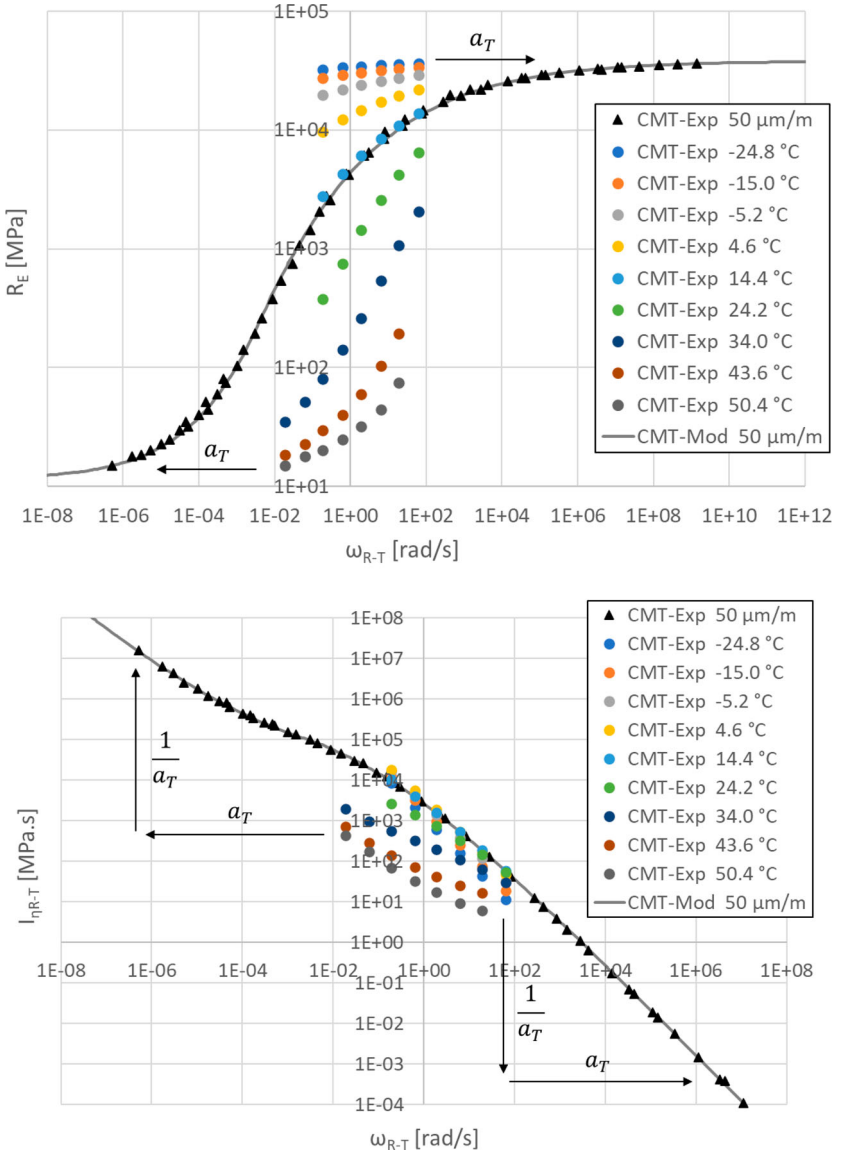

Figure 3. Phan's bituminous mixture – Sample E3550-5.1-0-1 (CMT, 50 µm/m). Plot of experimental data, application of the TTSP and fit with the VENoL(T,ω) model for the stiffness component $\Re_E$ (top) and the reduced viscosity component $\Im_{\eta,R-T}$ (bottom) function of the reduced pulsation ω_{R-T}.

Table 3. Phan's bituminous mixture. Modelling parameters of CY laws for the reference master curves $\Re_E(\omega_{R-T})$ and $\Im_{\eta,R-T}(\omega_{R-T})$ at $T_{ref} = 15°C$ and $\varepsilon_{0,ref} = 50\mu m/m$.

Transition reduced pulsation:		$\omega_{R-T,tr} = 3.00 \times 10^{-3}$rad/s	
$\Re_E(\omega_{R-T})$		$\Im_{\eta,R-T}(\omega_{R-T})$	
$\omega_{R-T} \leq \omega_{R-T,tr}$	$\omega_{R-T} \geq \omega_{R-T,tr}$	$\omega_{R-T} \leq \omega_{R-T,tr}$	$\omega_{R-T} \geq \omega_{R-T,tr}$
$R_{E,low,1} = 11.5MPa$	$R_{E,up,2} = 38,000$MPa	$I_{\eta,R-T,low,1} = 1.75 \times 10^4$ MPa s	$I_{\eta,R-T,up,2} = 6.70 \times 10^5$ MPa s
$\lambda_{E,R-T,1} = 1.11 \times 10^2$ s/rad	$\lambda_{E,R-T,2} = 1.00 \times 10^3$ s/rad	$\lambda_{\eta,R-T,1} = 2.78 \times 10^3$ s/rad	$\lambda_{\eta,R-T,2} = 4.00 \times 10^1$s/rad
$k_{E,1} = 0.307$	$k_{E,2} = -0.185$	$k_{\eta,1} = -0.250$	$k_{\eta,2} = 0.265$
$n_{E,1} = 2.630$	$n_{E,2} = 2.630$	$n_{\eta,1} = 0.070$	$n_{\eta,2} = -0.132$

4.1.2. Analytical modelling of $\Re_E(\omega_{R-T})$ and $\Im_{\eta,R-T}(\omega_{R-T})$

The previous experimental master curves are fitted with the CY laws (Equations (17) and (18)). The modelling parameters used for the sample E3550-5.1-0-1 are given Table 3. The fit of the components $\Re_E$ and $\Im_{\eta,R-T}$ seems correct (Figure 3, continuous curves), but to be certain of the result, it is necessary to check it in the Cole–Cole or Black spaces which are very sensitive to the parameters variation. The fit is correct in the Black space (Figure 4).

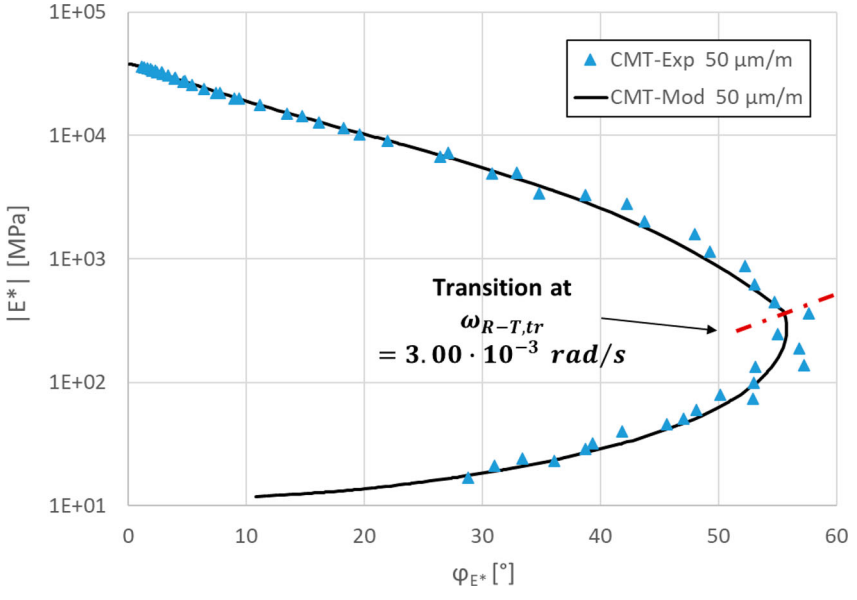

Figure 4. Phan's bituminous mixture – Sample E3550-5.1-0-1 (CMT, 50 µm/m). Plot of experimental data and fit with the VENoL(T,ω) model in the Black space.

4.2. Application of the VENoL model: addition of the influence of ε_0

The second major step in building the VENoL model consists of adding the strain amplitude influence to the VENoL(T,ω) model. This step is necessary because the CMTs are made at 50 µm/m while the CFTs are made at 100 µm/m. The new model designed is then called VENoL(T,ω,ε_0).

4.2.1. Identification of the TASSP factors laws

Setting up the TASSP using experimental NLTs data is not easy here. On the one hand, the number of nonlinearity experimental data is too small to be able to ensure the accuracy of the translation factors a_A and b_A found. The range of strain amplitudes is sufficient with 50, 75, 100 and 110 µm/m, but that of temperatures is too narrow with 8, 9.9, 11.9 and 13.8°C. On the other hand, the NLTs produced

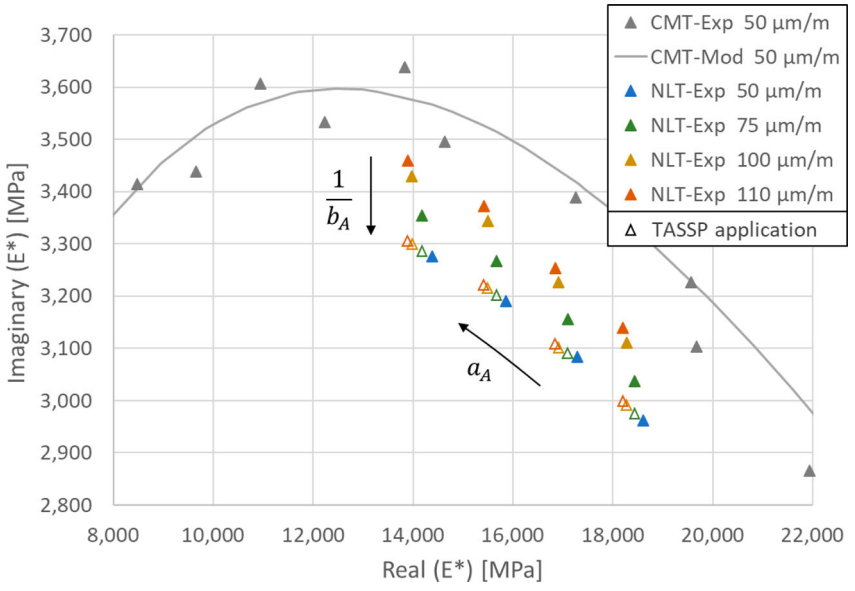

Figure 5. Phan's bituminous mixture – Sample E3550-5.1-0-1 (CMT, 50 µm/m) and sample E3550-5.1-0-6 (NLT, 50/75/100/110 µm/m). Plot of experimental data in the Cole-Cole space and comparison between CMT and NLTs (full marks). Application of the TASSP to the NLTs data to obtain a unique curve in the Cole–Cole space (empty marks).

Table 4. Phan's bituminous mixture. Average of the TASSP experimental translation factors $a_{A,exp}$ and $b_{A,exp}$ obtained after calculation according to the CMT at 50 µm/m and after normalisation depending on the NLT at 50 µm/m.

Reference	CMT 50 µm/m		NLT 50 µm/m	
ε_0 [µm/m]	$a_{A,calcul}$	$b_{A,calcul}$	$a_{A,exp}$	$b_{A,exp}$
NLT 50 µm/m	1.007	0.906	1.000	1.000
NLT 75 µm/m	0.933	0.925	0.927	1.021
NLT 100 µm/m	0.865	0.944	0.860	1.040
NLT 110 µm/m	0.840	0.951	0.834	1.047

at 50 µm/m do not overlap with the CMTs produced at 50 µm/m in the Cole–Cole space (Figure 5, blue and grey marks), whereas this, should be the case. It cannot be due to the specimens variability because the difference is too important, and the samples E3550-5.1-0-1 and E3550-5.1-0-6 were cut in the same slab. So, they have the same void percentage. In addition, the CMTs were carried out for two different specimens: E3550-5.1-0-1 and E3550-5.1-0-2 (the results of this second are not presented in this article). The results of these two specimens coincided perfectly in the Cole–Cole space.

The best hypothesis about the reason of this divergence could come from the time interval. The NLTs were carried out after the CMTs. Between them, some other tests were also carried out. In the meantime, it is possible that test bench settings have been changed. Therefore, this is not the CMT at 50 µm/m which is used as a reference to identify the TASSP coefficients as it should be, but the NLT at 50 µm/m.

By applying a couple of translation factors a_A and b_A to the results of the NLT at 50 µm/m, it is possible to find the results of another NLT at a different amplitude. Thus, for each strain amplitude and each data, a pair of experimental factors $a_{A,exp}$ and $b_{A,exp}$ must be defined. They can be estimated by applying the Equation (19) followed by Equation (20), obtained by isolating $a_{A,exp}$ and $b_{A,exp}$ in the Equations (17) and (18). However, the parameters of these two equations have been calibrated for the master curves obtained with the CMT at 50 µm/m. It is, therefore, necessary to normalise the translation factors calculated so that $a_{A,exp}$ and $b_{A,exp}$ are equal to 1.0 for the NLT at 50 µm/m. Then for each strain

Table 5. Phan's bituminous mixture. WLF-type laws parameters determining the evolution of the TASSP translation factors a_A and b_A.

Parameters	$a_{A,WLF}$	$b_{A,WLF}$
Reference amplitude [m/m]	$\varepsilon_{0,ref} = 5.00 \times 10^{-5}$	$\varepsilon_{0,ref} = 5.00 \times 10^{-5}$
Parameter 1 [–]	$C_{1,aA} = 0.590$	$C_{1,bA} = -0.106$
Parameter 2 [m/m]	$C_{2,aA} = 4.00 \times 10^{-4}$	$C_{2,bA} = 2.50 \times 10^{-4}$

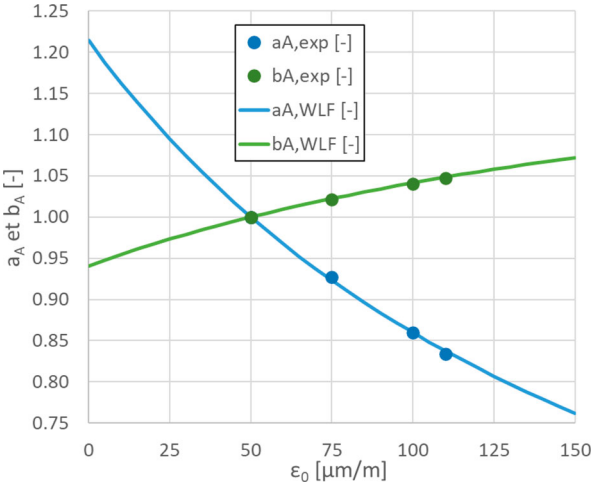

Figure 6. Phan's bituminous mixture. Variation of TASSP translation factors a_A and b_A according to the strain amplitude ε_0. Plot of the experimental factors and fit with WLF-type laws.

amplitude, an average of the calculated factors is done (Table 4). Because of results variability, some manually corrections could be necessary on this average to obtain a single reference curve.

By dividing the imaginary part of the complex stiffness modulus by the factor $b_{A,exp}$, a single curve is thus obtained in the Cole–Cole space (Figure 5, empty marks). All the points overlap on the NLT at 50 µm/m.

$$a_{A,exp} = \begin{cases} if\ \Re_{E,exp} \leq \Re_E(\omega_{R-TA,tr}), \\ \dfrac{1}{\lambda_{E,R-TA,1} \cdot \omega_{R-T,exp}} \cdot \left[\left[\dfrac{\Re_{E,exp}}{\Re_{E,low,1}} \right]^{\frac{k_{E,1}}{n_{E,1}-1}} - 1 \right]^{\frac{1}{k_{E,1}}} \\ - \\ if\ \Re_{E,exp} \geq \Re_E(\omega_{R-TA,tr}), \\ \dfrac{1}{\lambda_{E,R-TA,2} \cdot \omega_{R-T,exp}} \cdot \left[\left[\dfrac{\Re_{E,exp}}{\Re_{E,up,2}} \right]^{\frac{k_{E,2}}{n_{E,2}-1}} - 1 \right]^{\frac{1}{k_{E,2}}} \end{cases}, \tag{19}$$

$$b_{A,exp} = \begin{cases} if\ a_{A,exp} \cdot \omega_{R-T,exp} \leq \omega_{R-TA,tr}, \\ \dfrac{\Im_{\eta,R-T,exp}}{\Im_{\eta,R-TA,low,1} \cdot a_{A,exp}} \cdot \left[1 + \left[\lambda_{\eta,R-TA,1} \cdot a_{A,exp} \cdot \omega_{R-T,exp} \right]^{k_{\eta,1}} \right]^{-\frac{n_{\eta,1}-1}{k_{\eta,1}}} \\ - \\ if\ a_{A,exp} \cdot \omega_{R-T,exp} \geq \omega_{R-TA,tr}, \\ \dfrac{\Im_{\eta,R-T,exp}}{\Im_{\eta,R-TA,up,2} \cdot a_{A,exp}} \cdot \left[1 + \left[\lambda_{\eta,R-TA,2} \cdot a_{A,exp} \cdot \omega_{R-T,exp} \right]^{k_{\eta,2}} \right]^{-\frac{n_{\eta,2}-1}{k_{\eta,2}}} \end{cases}, \tag{20}$$

Evolution of the experimental translation factors $a_{A,exp}$ and $b_{A,exp}$ according to the strain amplitude is fitted with two WLF-type laws (Equations (12) and (13), Table 5 and Figure 6). Thus, the TASSP is created.

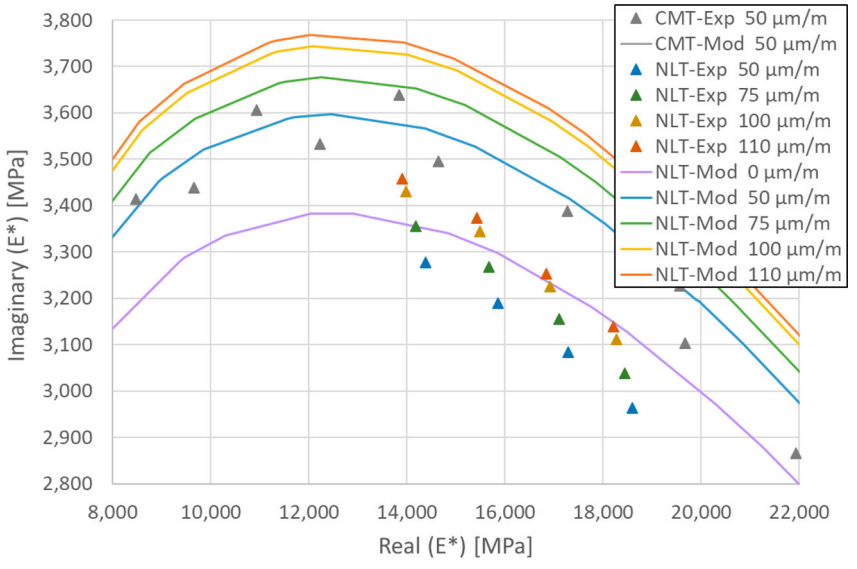

Figure 7. Phan's bituminous mixture – Sample E3550-5.1-0-1 (CMT, 50 µm/m) and sample E3550-5.1-0-6 (NLT, 50/75/100/110 µm/m). Plot of experimental data and fit with the VENoL(T,ω,ε_0) model in the Cole-Cole space. The curves 'CMT-Mod 50 µm/m' and 'NLT-Mod 50 µm/m' are logically overlaid.

4.2.2. Application of the TASSP to the VENoL model

The joint application of the VENoL model and the TTASSP makes it possible to obtain predictions of CMTs results at different strain amplitudes (Figure 7).

4.2.3. Discussion about the TASSP results

Despite problems encountered with the NLTs experimental data, the results show that the VENoL model building is flexible because it extracts the trend of NLTs to build the TASSP, which can be reused according to the reference CMT. Logically, the defined TASSP is biased but the error is minimised. However, the number of nonlinearity experimental data is too small, and the range of temperatures is too narrow to ensure the accuracy of the translation factors a_A and b_A calculated. For this last reason, the establishment of the TASSP cannot be confirmed. Other studies will be required.

4.3. Implementation of thixotropy in the VENoL model

The third and last step in building the VENoL model consists of adding the thixotropy influence to the VENoL(T,ω,ε_0) model. This step is necessary to predict the fatigue test. The model becomes the VENoL(T,ω,ε_0,N_{cycle}) model.

4.3.1. Assumption about evolution of thixotropy during a fatigue test

4.3.1.1. Decomposition of physical phenomena acting in fatigue. According to the experimental works and analyses in the literature on the separation of biasing and damaging effects, we can assume their evolution during a continuous fatigue test (Figure 8, top). Biasing effects could lead the Stages I and II of the fatigue curve, while damaging effects would increase slightly but gradually during these two stages. Then, the concentration of damage in certain areas would become too important leading to the development of macro-cracks and the rupture of the specimen (Stage III). These macro-cracks would break the continuity of the sample leading to a reduction of biasing effects. Indeed, with the presence of cracks, we think the imposed loading can no longer logically be transmitted to the whole

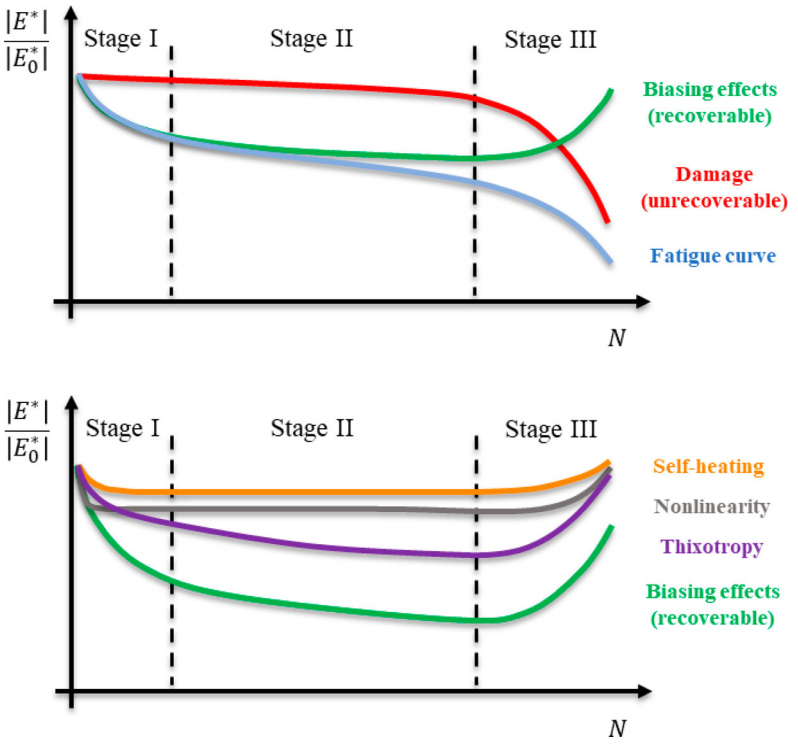

Figure 8. Assumption about the evolution of biasing and damaging effects composing a fatigue curve of the norm of the complex stiffness modulus (top) and decomposition of these biasing effects: nonlinearity, self-heating and thixotropy (bottom).

sample and certain regions would be less or no loaded (at rest). Biasing effects seem to be a consequence of viscosity which is sensitive to velocity. If velocity is no longer transmitted correctly through the cracked material, biasing effects would gradually disappear.

The curve of biasing effects can also be decomposed into three elements (Figure 8, bottom). The nonlinearity allows to observe the decrease in the norm of the complex stiffness modulus from 0 µm/m to the targeted strain amplitude. Its effect is situated only during the Stage I and stays constant during all the fatigue test until the rupture. The self-heating appears in Stage I. The increase in temperature decreases the norm of the complex stiffness modulus until a balance is reached between the dissipated energy and the thermal energy transferred to the external environment. During Stage II, balance is maintained. But in Stage III, macro-cracks appear, causing the fall of self-heating. Finally, the thixotropy corresponds to the remaining part of biasing effects and is the most important. Its impact on the decreasing of the norm of the complex stiffness modulus is significant in Stage I, then it slows down in Stage II before disappearing in Stage III.

4.3.1.2. How to model thixotropy?. In his article, Phan superimposed his fatigue tests with the CMT at 50 µm/m in the Cole–Cole and Black spaces of the complex stiffness modulus. Except for the nonlinear part and damage, the fatigue tests seem to follow the viscoelastic path of the CMT in the direction of a decrease in reduced pulsation.

To better understand this effect, we have superimposed these experimental results of CFTs (without the nonlinear part) and the CMT at 50 µm/m in the Black space of the complex viscosity modulus (Figure 9). The complex viscosity modulus is obtained by dividing the complex stress signal by the complex strain rate signal (Equations (21) and (22)). Each point of the CMT corresponding to a temperature–frequency pair, the isotherms (in grey, small dotted lines) and the isofrequencies (in brown, large dotted lines) can be plotted. This graph has the advantage of making influence of frequency and

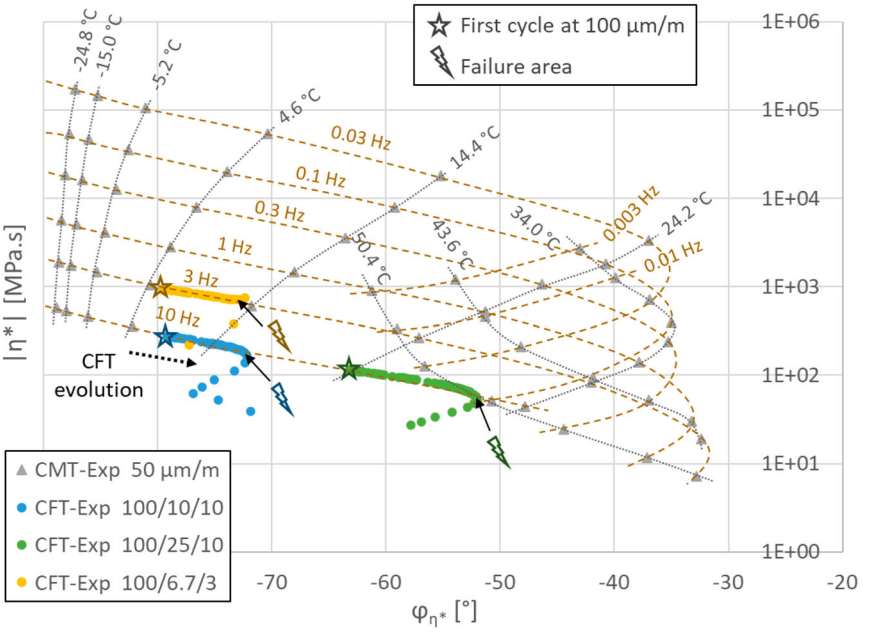

Figure 9. PHAN's bituminous mixture – Sample E3550-5.1-0-1 (CMT, 50 µm/m) and samples E3550-5.1-0-7/8/12 (CFT, 100 µm/m). Plot of experimental data in the Black space of the complex viscosity modulus and plot of isotherms and isofrequencies from the CMT. The CFTs are presented without the nonlinear part. As a reminder, the legend 100/10/10 corresponds to 100 µm/m/10°C/10 Hz.

temperature distinct.

$$\frac{\sigma^*(t)}{\dot{\varepsilon}^*(t)} = \eta^*(t), \tag{21}$$

$$\eta^*(t) = \frac{\Im(E^*)}{\omega} - i \cdot \frac{\Re(E^*)}{\omega}. \tag{22}$$

On this graph, it appears that Stages I and II of the three CFTs follow the path of isofrequencies in the direction of an increase in temperature until the break appears. Approximately equal to 10°C for the three CFTs, this apparent increase in temperature is not due to self-heating. Phan measured the surface temperature of test pieces during the fatigue tests, and the increase did not even exceed 1°C for the three samples E3550-5.1-0-7/8/12. It is simply the viscoelastic effect of thixotropy which acts in the same direction as an increase in temperature.

Equations (17) and (18) of the VENoL model define this viscoelastic path of the CMT at 50 µm/m. By applying the TASSP, this path can be known at 100 µm/m. Moreover, the passage from one temperature to another is modelled by the translation factor a_T (TTSP) and that from one amplitude to another by the factors a_A and b_A (TASSP). Their effects would be linked to viscosity, as it is the case for thixotropy. So, taking the example of the TASSP creation, the variations of two new translation coefficients a_X and b_X could be calculated. They would define the Time-thiXotropy Semi-Superposition Principle (TXSSP) and allow to model the thixotropic effect from one fatigue cycle to another.

4.3.1.3. How to distinguish the evolutionary trend of thixotropy from other effects?. *Nonlinear effect*: The TXSSP analysis will be performed on experimental data without the first part of CFTs, which consists to increase the axial strain amplitude progressively from 0 to the targeted amplitude of 100 µm/m over the first fifty cycles. During this step, several effects are acting, and we do not know if thixotropy can develop when strain amplitude is not stabilised. Moreover, the CFTs present exactly the same problem as the NLTs: in the Cole–Cole space, the values of the complex stiffness modulus

during the first cycles of the CFTs at 100 µm/m are located well below those from the CMT at 50 µm/m (Figure 13, top). Due to the variability of results, the few CFTs available and little biased, and a TASSP created from few data, it is difficult to analyse this part with precision. From these reasons and considering that thixotropic effect is not important over the first fifty cycles, we prefer to study it only when strain amplitude is stabilised at 100 µm/m.

Self-heating: It is difficult to separate with accuracy self-heating from thixotropy since the temperature field is not homogeneous in a sample during a fatigue test. But we know that this self-heating effect remains low for a small strain amplitude of 100 μm/m. So, to simplify this study, we can neglect it.

Damage: Section 4.3.1.1. teaches us that the thixotropic effect is predominant from phase I until about the half of phase II. From the middle of phase II, the decrease in the norm of the complex stiffness modulus as a function of the number of cycles seems generally to accelerate because the rate of damage evolution competes with that of thixotropy. Thus, an inflection in the evolution of the curves appears. Indeed, Figure 9 shows that the CFT curves seem no longer to follow the viscoelastic path of the CMT when the damage becomes too important. In phase III, the damage is predominant. Therefore, a change in the evolutionary trend of the shifts factors a_X and b_X (TXSSP) as a function of the number of cycles should be observed as damage begins to become predominant. By calibrating phase I and the first half of phase II, a mathematical trend could be defined for a_X and b_X representing the evolution of thixotropy. There may be damage in phase I and the first half of phase II, but its effect is considered negligible compared to that of thixotropy.

4.3.2. Use of the TXSSP and the TTAXSSP

4.3.2.1. TXSSP principle. The Time-thiXotropy Semi-Superposition Principle (TXSSP) connects thixotropy and pulsation. It is characterised by two translation factors a_X and b_X. The factor a_X is used to calculate the reduced pulsation ω_{R-X} and the reduced viscosity component $\Im_{\eta,R-X}$ (Equations (23) and (24)). The factor b_X is a correction coefficient that only affects $\Im_{\eta,R-X}$ (Equation (24)).

$$\omega_{R-X} = a_X \cdot \omega, \tag{23}$$

$$\Im_{\eta,R-X} = \frac{\Im_\eta}{a_X \cdot b_X}, \tag{24}$$

The thixotropic effect evolves during a fatigue test. Therefore, the factors a_X and b_X also vary according to the number of cycles performed N_{cycle}. The cycle zero, named N_0, is taken as the reference cycle, because at this stage the thixotropic effect has not started yet. It corresponds to the initial condition of CFTs. The factors a_X and b_X are equal to 1.0 at $N_{0,ref}$.

4.3.2.2. TTAXSSP principle. The combination of the TTSP, the TASSP and the TXSSP gives the Time-Temperature-Amplitude-thiXotropy Semi-Superposition Principle (TTAXSSP). It is characterised by the translation factors a_{TAX} and b_{AX} (Equations (25) and (26)). For the reference conditions, a_{TAX} and b_{AX} are equal to 1.0. The combination allows to calculate the reduced pulsation ω_{R-TAX} (Equation (27)) and to correct the reduced viscosity component $\Im_{\eta,R-TAX}$ (Equation (28)).

$$a_{TAX} = a_T \cdot a_A \cdot a_X, \tag{25}$$

$$b_{AX} = b_A \cdot b_X, \tag{26}$$

$$\omega_{R-TAX} = a_{TAX} \cdot \omega, \tag{27}$$

$$\Im_{\eta,R-TAX} = \frac{\Im_\eta}{a_{TAX} \cdot b_{AX}}. \tag{28}$$

The parameters names resulting from CY laws defining the stiffness and viscosity components $\Re_E$ and $\Im_\eta$ evolve but their values remain the same since a_{TAX} and b_{AX} are equal to 1.0 (Table 6).

Table 6. VENoL($T,\omega,\varepsilon_0,N_{cycle}$) model. Evolution of the parameters naming of CY laws defining the stiffness and viscosity components $\Re_E$ and $\Im_\eta$ according to the principle used (improvement of Table 1).

Parameters	TTSP	TTASSP	TTAXSSP
Transition reduced pulsation [rad/s]	$\omega_{R-T,tr}$	$\omega_{R-TA,tr}$	$\omega_{R-TAX,tr}$
Stiffness component – Parameter 1 controlling the position of the curve on the axis ω [s/rad]	$\lambda_{E,R-T,1}$	$\lambda_{E,R-TA,1}$	$\lambda_{E,R-TAX,1}$
Stiffness component – Parameter 2 controlling the position of the curve on the axis ω [s/rad]	$\lambda_{E,R-T,2}$	$\lambda_{E,R-TA,2}$	$\lambda_{E,R-TAX,2}$
Viscosity component – Lower bound [MPa s]	$\Im_{\eta,R-T,low,1}$	$\Im_{\eta,R-TA,low,1}$	$\Im_{\eta,R-TAX,low,1}$
Viscosity component – Parameter 1 controlling the position of the curve on the axis ω [s/rad]	$\lambda_{\eta,R-T,1}$	$\lambda_{\eta,R-TA,1}$	$\lambda_{\eta,R-TAX,1}$
Viscosity component – Upper bound [MPa s]	$\Im_{\eta,R-T,up,2}$	$\Im_{\eta,R-TA,up,2}$	$\Im_{\eta,R-TAX,up,2}$
Viscosity component – Parameter 2 controlling the position of the curve on the axis ω [s/rad]	$\lambda_{\eta,R-T,2}$	$\lambda_{\eta,R-TA,2}$	$\lambda_{\eta,R-TAX,2}$

4.3.3. Identification of the TXSSP factors laws

The CMT at 15°C and 50 µm/m becomes the frame of reference of the TTAXSSP. Because the study is executed without the nonlinear part of CFTs, the cycle N_0 is therefore the first cycle for which the fatigue amplitude of 100 µm/m has been reached. The TASSP allows the transition from the CMT at 50 µm/m to the NLT at 100 µm/m, which is considered as the initial condition of CFTs at 100 µm/m.

Evolution of the experimental translation factors $a_{X,exp}$ and $b_{X,exp}$ according to the number of cycles is estimated using the Equations (29) and (30), defined by isolating $a_{X,exp}$ and $b_{X,exp}$ in the Equations (17) and (18). These equations are applied to CFTs at 100 µm/m carried out on samples E3550-5.1-0-7/8/12.

$$a_{X,exp} = \begin{cases} if\ \Re_{E,exp} \le \Re_E(\omega_{R-TAX,tr}), \\ \frac{1}{\lambda_{E,R-TAX,1}\cdot\omega_{R-TA,exp}} \cdot \left[\left[\frac{\Re_{E,exp}}{\Re_{E,low,1}}\right]^{\frac{k_{E,1}}{n_{E,1}-1}} - 1\right]^{\frac{1}{k_{E,1}}} \\ ---------- \\ if\ \Re_{E,exp} \ge \Re_E(\omega_{R-TAX,tr}), \\ \frac{1}{\lambda_{E,R-TAX,2}\cdot\omega_{R-TA,exp}} \cdot \left[\left[\frac{\Re_{E,exp}}{\Re_{E,up,2}}\right]^{\frac{k_{E,2}}{n_{E,2}-1}} - 1\right]^{\frac{1}{k_{E,2}}} \end{cases}, \tag{29}$$

$$b_{X,exp} = \begin{cases} if\ a_{X,exp}\cdot\omega_{R-TA,exp} \le \omega_{R-TAX,tr}, \\ \frac{\Im_{\eta,R-TA,exp}}{\Im_{\eta,R-TAX,low,1}\cdot a_{X,exp}} \cdot [1 + [\lambda_{\eta,R-TAX,1}\cdot a_{X,exp}\cdot\omega_{R-TA,exp}]^{k_{\eta,1}}]^{-\frac{n_{\eta,1}-1}{k_{\eta,1}}} \\ ---------- \\ if\ a_{X,exp}\cdot\omega_{R-TA,exp} \ge \omega_{R-TAX,tr}, \\ \frac{\Im_{\eta,R-TA,exp}}{\Im_{\eta,R-TAX,up,2}\cdot a_{X,exp}} \cdot [1 + [\lambda_{\eta,R-TAX,2}\cdot a_{X,exp}\cdot\omega_{R-TA,exp}]^{k_{\eta,2}}]^{-\frac{n_{\eta,2}-1}{k_{\eta,2}}} \end{cases}, \tag{30}$$

The results obtained for $a_{X,exp}(N_{cycle})$ and $b_{X,exp}(N_{cycle})$ are presented in Figure 10, after normalisation of the values according to $a_{X,exp}(N_0)$ and $b_{X,exp}(N_0)$. Indeed, theoretically, $a_{X,exp}(N_0)$ and $b_{X,exp}(N_0)$ are supposed to be equal to 1.0 but the experimental reality is different. On the one hand, results in dispersion can lead to values of $a_{X,exp}$ and $b_{X,exp}$ approaching for example 0.90 or 1.20 for the 'zero' cycle. On the other hand, as we said before, the CFTs present the same problem as the NLTs and are therefore a bit biased. This adds an additional divergence. To be able to compare the tests with each other, it is, therefore, a good idea to apply this normalisation.

By analysing the curves of $a_{X,exp}$ and $b_{X,exp}$ obtained for each CFT, it turns out that they are remarkably close to each other. An average of these three curves is calculated for $a_{X,exp}$ and $b_{X,exp}$.

An inflection of average experimental curves seems to appear around 100,000 cycles (Figure 11), possibly due to the damage becoming predominant as we said it in the section 4.3.1.3. Therefore, by

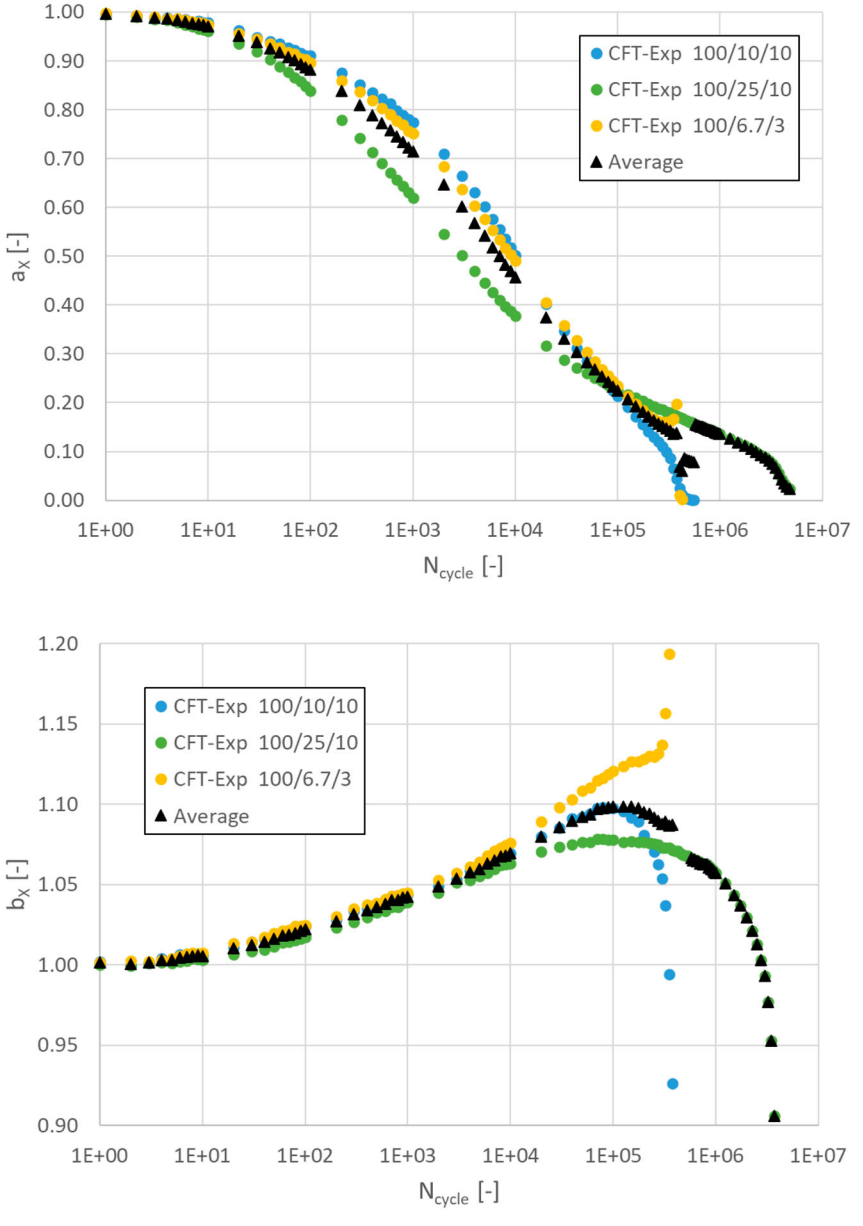

Figure 10. Phan's bituminous mixture – Samples E3550-5.1-0-7/8/12 (CFT, 100 µm/m). Variation of the experimental translation factors $a_{X,exp}$ (top) and $b_{X,exp}$ (bottom) from the TXSSP after normalisation according to the number of cycles N_{cycle} for each sample and their average. As a reminder, the legend 100/10/10 corresponds to 100 µm/m/10°C/10 Hz.

calibrating only the mathematical trend of these two average experimental curves before the inflection point, an evolution of thixotropy can be obtained since predominant, it orients the shape of the curve. We have considered that the damage effect is negligible compared to that of thixotropy in this part.

These averages can be calibrated with Carreau–Yasuda-type laws, which make it possible to represent sigmoid in a logarithmic coordinate system (Equations (31) and (32)). The denominations and values of the parameters used are given in Table 7. Thus, the evolution laws a_X and b_X form the

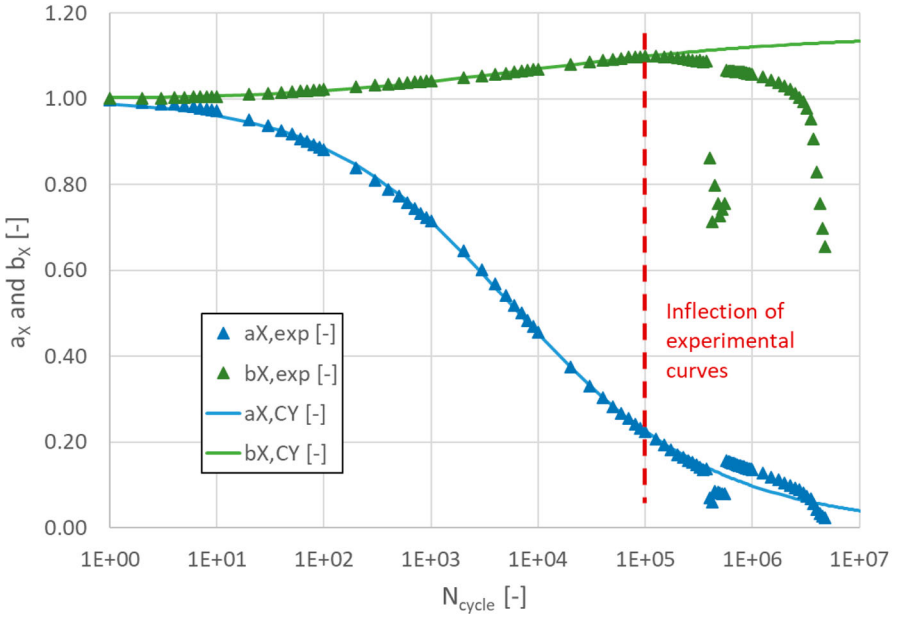

Figure 11. Phan's bituminous mixture. Variation of the translation factors a_X and b_X from the TXSSP according to the number of cycles N_{cycle}. Plot of the averages of experimental factors and fit with CY-type laws.

Table 7. Phan's bituminous mixture. The CY-type laws parameters determining the evolution of TXSSP translation factors a_X and b_X.

Parameters	$a_{X,CY}$	$b_{X,CY}$
Lower bound [–]	none	$b_{X,\,low} = 1.00$
Upper bound [–]	$a_{X,\,up} = 1.00$	$b_{X,\,up} = 1.15$
Position of the curve on the axis N_{cycle} [N_{cycle}^{-1}]	$\lambda_{aX} = 3.00 \times 10^{-4}$	$\lambda_{bX} = 1.30 \times 10^{-3}$
Slope/bound transition parameter [–]	$k_{aX} = 0.51$	$k_{bX} = -0.30$
Slope parameter [–]	$n_{aX} = 0.60$	$n_{bX} = 1.60$

thixotropic effect acting in fatigue.

$$a_X(N_{\text{cycle}}) = a_{X,\,up} \cdot [1 + [\lambda_{aX} \cdot N_{cycle}]^{k_{aX}}]^{\frac{n_{aX}-1}{k_{aX}}}$$
$$k_{aX} > 0; n_{aX} < 1; a_{X,up} = 1.0 \tag{31}$$

$$b_X(N_{\text{cycle}}) = b_{X,\,low} + (b_{X,\,up} - b_{X,\,low}) \cdot [1 + [\lambda_{bX} \cdot N_{\text{cycle}}]^{k_{bX}}]^{\frac{n_{bX}-1}{k_{bX}}}$$
$$k_{bX} < 0; n_{bX} > 1; b_{X,low} = 1.0. \tag{32}$$

4.3.4. Application of the TXSSP to the VENoL(T,ω,ε_0) model

The comparison of Stages I and II of experimental CFTs with their associated analytical modelling of ThiXotropy (TX) must allow to verify the conformity of the evolution laws of the factors a_X and b_X. Therefore, the stiffness and viscosity components $\Re_E$ and $\Im_\eta$ of the VENoL model associated with the TTAXSSP are calculated at 100 µm/m. No law of damage has been added to the modelling.

From the calculated couples $\Re_E$ and $\Im_\eta$, the norm of the complex stiffness modulus $|E^*|$ and the phase angle φ_{E^*} as a function of the number of cycles is deduced (Figure 12). The Stages I and II of the three experimental CFTs are faithfully reproduced by the VENoL($T,\omega,\varepsilon_0,N_{\text{cycle}}$) model. The TX curves modelled at 10°C, 10 Hz and 6.7°C, 3 Hz are overlaid because the two tests have the same reduced

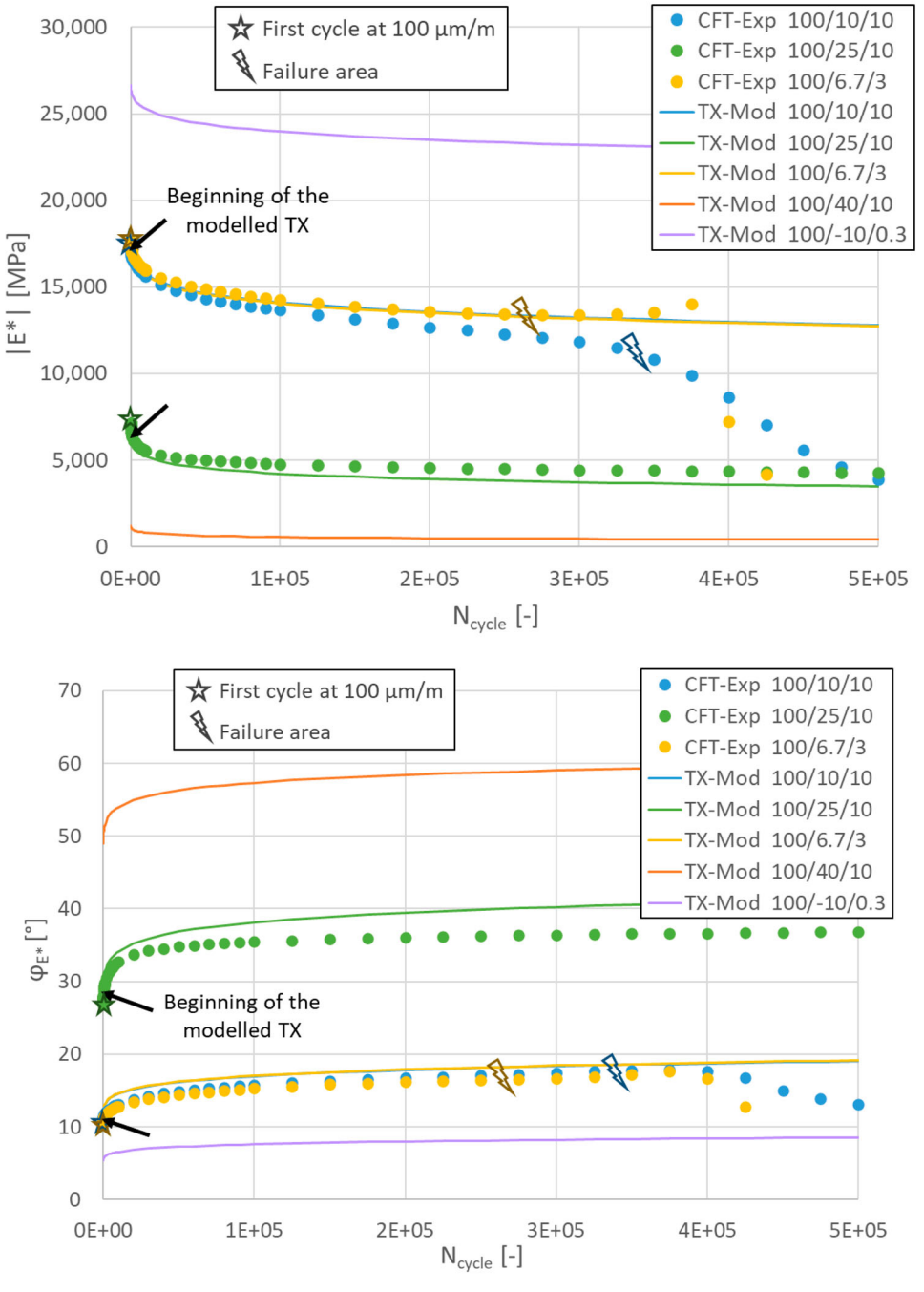

Figure 12. Phan's bituminous mixture – Samples E3550-5.1-0-7/8/12 (CFT, 100 µm/m). Variation of the norm of the complex stiffness modulus $|E^*|$ (top) and of the phase angle φ_{E^*} (bottom) according to the number of cycles N_{cycle}. Plot of experimental data (CFT) and of the VENoL($T,\omega,\varepsilon_0,N_{cycle}$) model (TX). The blue and yellow curves are overlaid. As a reminder, the legend 100/10/10 corresponds to 100 µm/m/10°C/10 Hz.

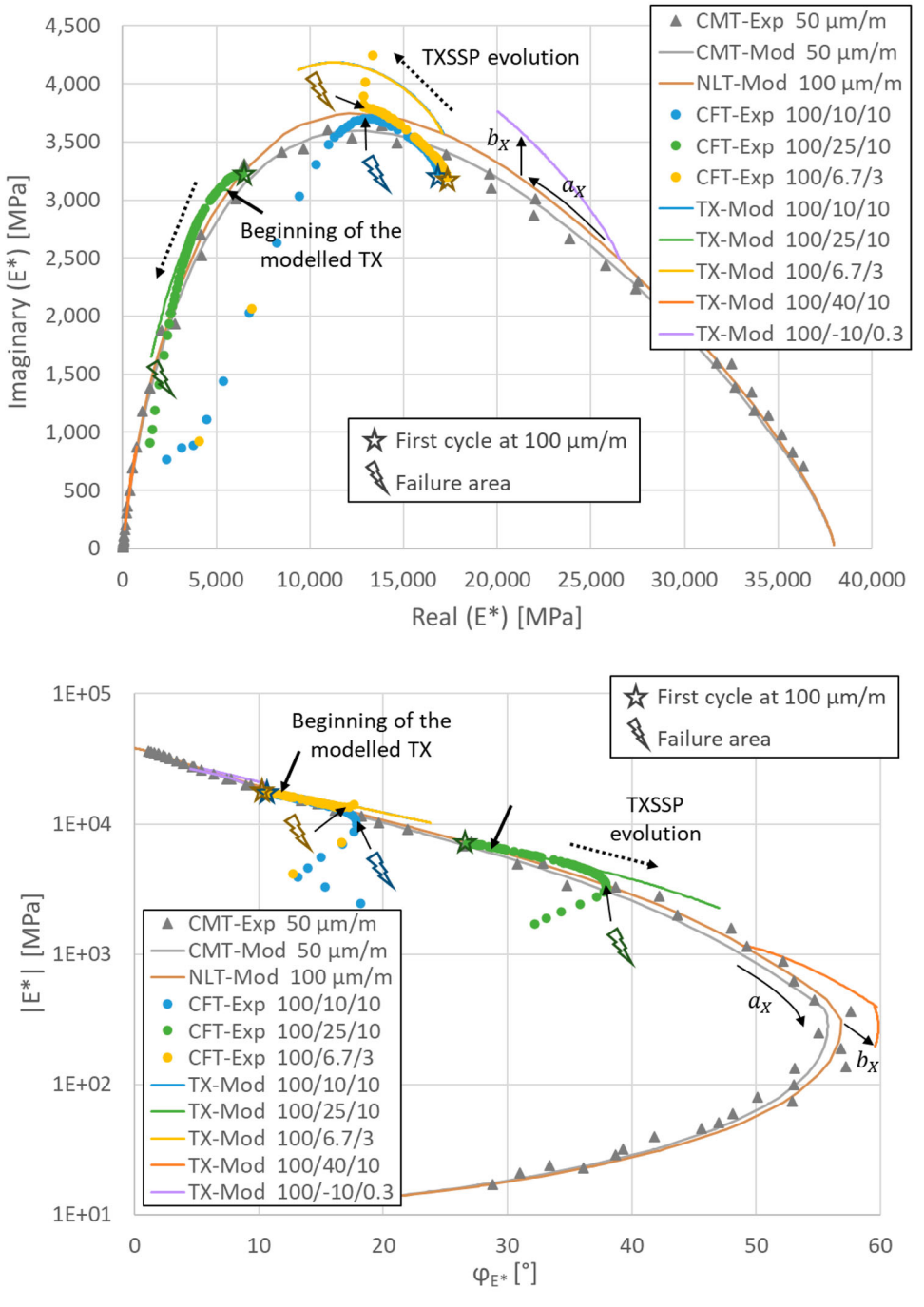

Figure 13. Phan's bituminous mixture – Sample E3550-5.1-0-1 (CMT, 50 µm/m) and samples E3550-5.1-0-7/8/12 (CFT, 100 µm/m). Plot of experimental data and of the VENoL(T,ω,ε_0,N_{cycle}) model in the Cole–Cole space (top) and in the Black space (bottom). The blue and yellow curves are overlaid. As a reminder, the legend 100/10/10 corresponds to 100 µm/m/10°C/10 Hz.

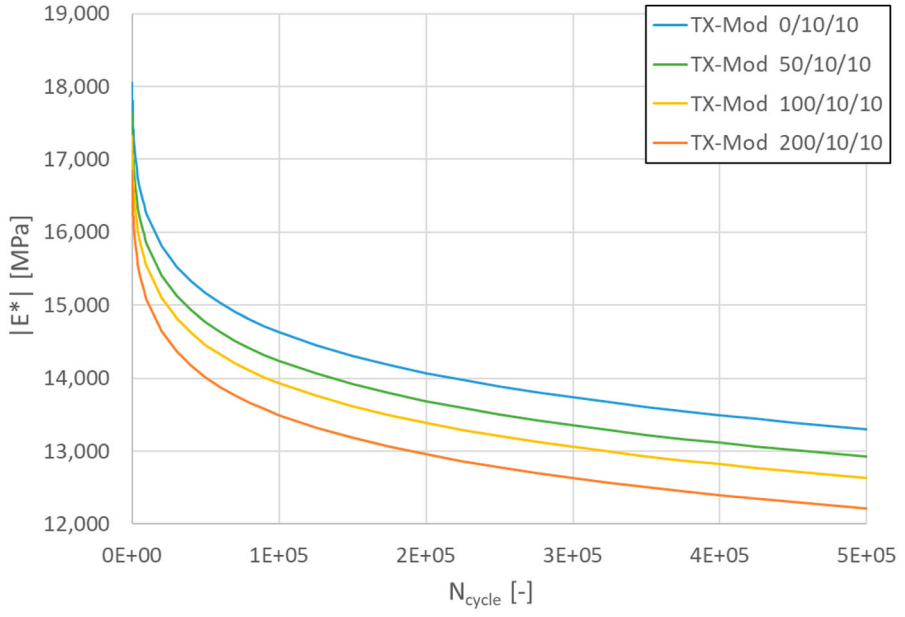

Figure 14. Application of the VENoL(T,ω,ε_0,N_{cycle}) model with the Phan's bituminous mixture. Variation of the norm of the complex stiffness modulus according to the number of cycles N_{cycle} for TXs modelled at 10°C, 10 Hz and four different strain amplitudes: 0, 50, 100 and 200 µm/m.

pulsation at TTSP. Two TXs at 40°C, 10 Hz and −10°C, 0.3 Hz are modelled in addition to assess the evolution of Stages I and II according to temperature and frequency. To issue a critical opinion, there is a slight difference between the experimentation and the modelling at the level of the initial condition which logically carries over to the entire curve.

This difference is particularly visible in the Cole–Cole space (Figure 13, top). The experimental CFTs at 10°C, 10 Hz and 6.7°C, 3 Hz, whose amplitudes are 100 µm/m, start below the CMT at 50 µm/m when they should start around the NLT modelled at 100 µm/m. Hence this deviation from the initial condition. This problem has already been mentioned in Section 4.3.3. Besides this point, the modelled TXs faithfully reproduce the shape of Stages I and II of experimental CFTs in the Cole–Cole and Black spaces (Figure 13).

4.3.5. Discussion about the TXSSP results

The TXSSP has been investigated for only three experimental CFTs. More data will therefore be needed to confirm or infirm the tendencies observed on a_X and b_X.

Furthermore, the separation of self-heating from thixotropy in the TXSSP was not studied here because the self-heating did not even exceed 1°C for the three samples E3550-5.1-0-7/8/12. It is true that Phan made temperature measurements at the surface and in the centre of specimens, but they are local measurements. To take this into account, it would be necessary to know the average self-heating effect over the entire specimen. Therefore, some other CFTs with higher strain amplitudes than 100 µm/m, that is, higher self-heating, would be interesting to evaluate this interaction.

The three CFTs were also executed for the same strain amplitude at 100 µm/m. As shown in Figure 14, regardless of the amplitude level, the norm of the modelled complex stiffness modulus decreases in the same way as a function of the number of cycles, even for 0 µm/m. This is not correct since the Wöhler curve indicates that the lifetime of an asphalt concrete increases with the decrease in amplitude. Thus, the effect of the strain amplitude does not seem to intervene only on the initial condition of TXSSP coefficients but also on their variation according to the number of cycles. Finally, this TXSSP gives results only at an imposed strain amplitude. More CFTs at different strain amplitudes would be also necessary to estimate this interaction.

Physical property	Symbol		Type of law	Nb param.
Stiffness component	$\Re_E$	$\omega_{R-TAX} \leq \omega_{R-TAX,tr}$	CY law	4
		$\omega_{R-TAX} \geq \omega_{R-TAX,tr}$	CY law	4
Viscosity component	$\Im_\eta$	$\omega_{R-TAX} \leq \omega_{R-TAX,tr}$	CY law	4
		$\omega_{R-TAX} \geq \omega_{R-TAX,tr}$	CY law	4
Influencing viscoelasticity:				
• signal pulsation ω				
• temperature T	TTSP	a_T	WLF law	2
• strain amplitude ε_0	TASSP	a_A b_A	WLF law	2 + 2 = 4
• cycles N_{cycle} (thixotropy)	TXSSP	a_X b_X	CY law	3 + 4 = 7
	TTAXSSP	a_{TAX} b_{AX}		

Figure 15. Summary of the VENoL(T,ω,ε_0,N_{cycle}) model.

A summary of the structure of the VENoL(T,ω,ε_0,N_{cycle}) model is given in Figure 15. By adding the TXSSP parameters, now the model includes 29 parameters. This is a significant number but once these parameters have been defined for the studied asphalt concrete, they remain fixed. Furthermore, it seems difficult to macroscopically model the effects of temperature, strain amplitude and the number of cycles other than by using principles composing the TTAXSSP. In addition, depending on the desired modelling, it may not be necessary to use each law.

5. Conclusion

An inventory of the literature evoking thixotropy has been carried out to better understand its role during a cyclic fatigue test on asphalt concrete.

- It appears that it is only a biasing effect because the loss of rigidity that it causes is recoverable when the fatigue test is stopped.
- From this research, we also assume that under the thixotropic effect, the stiffness decreases rapidly in Stage I, then slowly but continuously in Stage II before the effect is gradually annihilated after the appearance of macro-cracks in Stage III breaking the continuity of the test piece.
- In addition, we have observed during the Stages I and II of a CFT that the thixotropic effect follows the viscoelastic path of the CMT. Its evolution is equivalent to an increase in temperature. Viscosity seems to guide thixotropy. When the damage becomes predominant, the CFT curve takes another direction.

Inspired by the TTSP and the TASSP, a new superposition principle has been therefore developed to model thixotropy during a fatigue test, the TXSSP.

- It is characterised by two translation factors a_X and b_X. Their evolutions are defined by Carreau–Yasuda-type laws and depend on the number of cycles. The zero cycle, the initial condition, represents the frame of reference.
- These translation factors a_X and b_X affect the stiffness and viscosity components $\Re_E$ and $\Im_\eta$ of the VENoL model so that they evolve as the fatigue test progresses.
- The methodology of this principle consists of determining a trend common to several fatigue tests of different temperatures and frequencies in order to calibrate it and reintroduce it into the VENoL model. Thus, the model links the instantaneous rheological behaviour of asphalt concrete and the fatigue behaviour (thixotropy).

The application of the TXSSP with Phan's experimental data has been checked.

- With the combined application of the VENoL model and the TXSSP, it has been possible to reproduce analytically at a targeted amplitude with a single set of parameters for a_X and b_X the experimental evolution of the thixotropic effect during a fatigue test for different couples of temperatures and frequencies.
- But this way of proceeding also includes self-heating part in the modelled thixotropy. Moreover, assumptions have been made to define the evolutions of thixotropy and damage based on experimental works and analyses found in literature about the quantification of biasing and damaging effects in fatigue.

Acknowledgements

The authors warmly thank the authors Cong Viet Phan, Hervé Di Benedetto, Cédric Sauzéat, Josselin Dade and Simon Pouget for kindly providing their experimental data presented in their article (Phan et al., 2017a).

Disclosure statement

No potential conflict of interest was reported by the author(s).

Funding

The work presented in this article was supported by the French institution Agence Nationale de la Recherche (ANR, eng: National Agency for Research) (ANR-MoveDVDC project, ref. ANR-17-CE22-0014-03).

References

Baaj, H. (2002). *Comportement à la fatigue des matériaux granulaires traités aux liants hydrocarbonés* [Ph. D. thesis]. ENTPE, Lyon, France, 266 p. (in French).

Baaj, H., Mikhailenko, P., Almutairi, H., & Di Benedetto, H. (2018). Recovery of asphalt mixture stiffness during fatigue loading rest periods. *Construction and Building Materials*, *158*, 591–600. https://doi.org/10.1016/j.conbuildmat.2017.10.016

Babadopulos, L. F. d. A. L., Orozco, G., Sauzéat, C., & Di Benedetto, H. (2019). Reversible phenomena and fatigue damage during cyclic loading and rest periods on bitumen. *International Journal of Fatigue*, *124*, 303–314. https://doi.org/10.1016/j.ijfatigue.2019.03.008

Bodin, D., Pijaudier-Cabot, G., de La Roche, C., Piau, J.-M., & Chabot, A. (2004). Continuum damage approach to asphalt concrete fatigue modeling. *Journal of Engineering Mechanics*, *130*(6), 700–708. https://doi.org/10.1061/(ASCE)0733-9399-(2004)130:6(700)

Botella, R., Pérez-Jiménez, F. E., López-Montero, T., & Miró, R. (2020). Cyclic testing setups to highlight the importance of heating and other reversible phenomena on asphalt mixtures. *International Journal of Fatigue*, *134*, 105514. https://doi.org/10.1016/j.ijfatigue.2020.105514

Byron Bird, R., & Carreau, J. P. (1968). A nonlinear viscoelastic model for polymer solutions and melts—I. *Chemical Engineering Science*, *23*(5), 427–434. https://doi.org/10.1016/0009-2509(68)87018-6

Castro, M., & Sanchez, J. A. (2007). Damage based model for prediction of asphalt concrete fatigue curves. *Journal of Materials in Civil Engineering*, *19*(8), 700–702. https://doi.org/10.1061/(ASCE)0899-1561(2007)19:8(700)

Christensen, D. W., & Bonaquist, R. (2012). Modeling of fatigue damage functions for hot mix asphalt and application to surface cracking. *Road Materials and Pavement Design*, *13*(1), 102–123. https://doi.org/10.1080/14680629.2012.657029

Coulon, L. (2022). *Modélisation de l'effet du vieillissement et de la fatigue sur le comportement résiduel des matériaux de chaussées* [Unpublished PhD thesis]. INSA Strasbourg, France (in French).

Coulon, L., Koval, G., Chazallon, C., & Roux, J.-N. (2021a). Modeling of T/C complex stiffness modulus test and nonlinearity of asphalt concrete mixes. *Proceedings of the Rilem International Symposium on Bituminous Materials*, *27*(171), doi:10.1007/978-3-030-46455-4_171

Coulon, L., Koval, G., Chazallon, C., & Roux, J.-N. (2021b). Analytical modelling of T/C complex stiffness modulus tests and nonlinearity of asphalt concrete. Reviewed by *Road Materials and Pavement Design* since 2021-3-18.

Di Benedetto, H., de la Roche, C., Baaj, H., Pronk, A. C., & Lundström, R. (2004). Fatigue of bituminous mixtures. *Materials and Structures*, *37*(3), 202–216. https://doi.org/10.1007/BF02481620

Di Benedetto, H., Nguyen, Q. T., & Sauzéat, C. (2011). Nonlinearity, heating, fatigue and thixotropy during cyclic loading of asphalt mixtures. *Road Materials and Pavement Design*, *12*(1), 129–158. https://doi.org/10.1080/14680629.2011.9690356

Graziani, A., Cardone, F., Virgili, A., & Canestrari, F. (2019). Linear viscoelastic characterisation of bituminous mixtures using random stress excitations. *Road Materials and Pavement Design*, *20*(1), S390–S408. https://doi.org/10.1080/14680629.2019.1587494

Hernandez-Fernandez, N., Underwood, B. S., & Ossa-Lopez, A. (2020). Simulation of the asphalt concrete stiffness degradation using simplified viscoelastic continuum damage model. *International Journal of Fatigue*, *140*, 105850. https://doi.org/10.1016/j.ijfatigue.2020.105850

Hou, T. (2009). *Fatigue performance prediction of North Carolina mixtures using simplified viscoelastic continuum damage model* [Ph. D. thesis]. North Carolina State University, Raleigh, USA, 132 p.

Isailović, I., Wistuba, M. P., & Cannone Falchetto, A. (2017). Influence of rest period on asphalt recovery considering nonlinearity and self-heating. *Construction and Building Materials*, *140*, 321–327. https://doi.org/10.1016/j.conbuildmat.2017.02.122

IUPAC. (1997). Compendium of Chemical Terminology, 2nd ed. (the "Gold Book"). Compiled by McNaught, A. D. and Wilkinson, A. *Blackwell Scientific Publications*, Oxford (1997). Online version (2019-) created by Chalk, S. J. ISBN 0-9678550-9-8. https://doi.org/10.1351/goldbook

Lee, H. J., Daniel, J. S., & Kim, Y. R. (2000). Continuum damage mechanics-based fatigue model of asphalt concrete. *Journal of Materials in Civil Engineering*, *12*(2), 105–112. https://doi.org/10.1061/(ASCE)0899-1561(2000)12:2(105)

Liu, G. (2019). *Discrete element modelling of asphalt concrete reinforced with fiber glass grids* [Ph. D. thesis]. INSA Strasbourg, France, 204 p.

Lv, S., Hu, L., Xia, C., Wang, X., Borges Cabrera, M., Guo, S., & Chen, J. (2020). Development of fatigue damage model of asphalt mixtures based on small-scale accelerated pavement test. *Construction and Building Materials*, *260*, 119930. https://doi.org/10.1016/j.conbuildmat.2020.119930

Mangiafico, S. (2014). *Linear viscoelastic properties and fatigue of bituminous mix-tures produced with Reclaimed Asphalt Pavement and corresponding binder blends* [Ph. D. thesis]. ENTPE, Lyon, France, 318 p.

Mangiafico, S., Sauzéat, C., Di Benedetto, H., Pouget, S., Olard, F., & Planque, L. (2015). Quantification of biasing effects during fatigue tests on asphalt mixes: Non-linearity, self-heating and thixotropy. *Road Materials and Pavement Design*. https://doi.org/10.1080/14680629.2015.1077000

Mewis, J., & Wagner, N. J. (2009). Thixotropy. *Advances in Colloid and Interface Science*, *147-148*, 214–227. https://doi.org/10.1016/j.cis.2008.09.005

Mouillet, V., De La Roche, C., Chailleux, E., & Coussot, P. (2012). Thixotropic behavior of paving-grade bitumens under dynamic shear. *Journal of Materials in Civil Engineering*, *24*(1), 23–31. https://doi.org/10.1061/(ASCE)MT.1943-5533.0000354

Nguyen, Q. T., Di Benedetto, H., & Sauzéat, C. (2015). Linear and nonlinear viscoelastic behaviour of bituminous mixtures. *Materials and Structures*, *48*(7), 2339–2351. https://doi.org/10.1617/s11527-014-0316-5

Pérez-Jiménez, F. E., Botella, R., & Miró, R. (2012). Differentiating between damage and thixotropy in asphalt binder's fatigue tests. *Construction and Building Materials*, *31*, 212–219. https://doi.org/10.1016/j.conbuildmat.2011.12.098

Phan, C. V., Di Benedetto, H., Sauzéat, C., Dayde, J., & Pouget, S. (2017a). Quantification of different effects occurring during fatigue tests on bituminous mixtures. *Fatigue and Fracture of Engineering Materials and Structures*, 1–14. https://doi.org/10.1111/ffe.12646

Phan, C. V., Di Benedetto, H., Sauzéat, C., Lesueur, D., Pouget, S., Olard, F., & Dupriet, S. (2017b). Complex modulus and fatigue resistance of bituminous mixtures containing hydrated lime. *Construction and Building Materials*, *139*, 24–33. https://doi.org/10.1016/j.conbuildmat.2017.02.042

Riahi, E., Allou, F., Botella, R., Fakhari Tehrani, F. F., Dubois, F., Absi, J., Petit, C., & Pérez-Jiménez, F. E. (2017). Modelling self-heating and thixotropy phenomena under the cyclic loading of asphalt. *Road Materials and Pavement Design*, *18*(2), 155–163. https://doi.org/10.1080/14680629.2017.1305145

Schapery, R. A. (1969). On the characterization of nonlinear viscoelastic materials. *Polymer Engineering and Science*, *9*(4), 295–310. https://doi.org/10.1002/pen.760090410

Shan, L. Y., Tan, Y. Q., Underwood, B. S., & Kim, Y. R. (2011). Separation of thixotropy from fatigue process of asphalt binder. *Transportation Research Record: Journal of the Transportation Research Board*, *2207*(1), 89–98. https://doi.org/10.3141/2207-12

Underwood, B. S., & Kim, Y. R. (2013). Nonlinear viscoelastic behavior of asphalt concrete and its implication for fatigue modeling. *Transportation Research Record: Journal of the Transportation Research Board*, *2373*(1), 100–108. https://doi.org/10.3141/2373-11

Williams, M. L., Landel, R. F., & Ferry, J. D. (1955). The temperature dependence of relaxation mechanisms in amorphous polymers and other glass-forming liquids. *Journal of the American Chemical Society*, *77*(14), 3701–3707. https://doi.org/10.1021/ja01619a008

Yasuda, K. (1979). *Investigation of the analogies between viscometric and linear viscoelastic properties of polystyrene fluids* [Ph. D. thesis]. MIT, Cambridge, USA, 587 p.

Zeng, M. (1997). *Nonlinear viscoelastic behaviour of asphalt concrete in stress relaxation* [Ph.D. thesis]. University of Manitoba, Winnipeg, Canada, 248 p.

Zeng, M., Bahia, H. U., Zhai, H., Anderson, M. R., & Turner, P. (2001). Rheological modeling of modified asphalt binders and mixtures. *Journal of the Association of Asphalt Paving Technologists*, *70*, 403–441.